Solid State Electronics xxx (xxxx) xxxx

Contents lists available at ScienceDirect

Solid State Electronics

journal homepage: www.elsevier.com/locate/sse

# Scaled resistively-coupled $VO_2$ oscillators for neuromorphic computing

Elisabetta Corti[a,b], Bernd Gotsmann[a], Kirsten Moselund[a], Adrian M. Ionescu[b], John Robertson[c], Siegfried Karg[a,*]

[a] IBM Research – Zurich, Rüschlikon, Switzerland
[b] Nanoelectronic Devices Laboratory, École Polytechnique Fédérale de Lausanne, Lausanne, Switzerland
[c] Department of Engineering, University of Cambridge, Cambridge, United Kingdom

ARTICLE INFO

The review of this paper was arranged by "Joris Lacord"

*Keywords:*
Neuromorphic computing
Coupled oscillators
$VO_2$
Image recognition
Timing
Phase
Resistive-coupling

ABSTRACT

New computation schemes inspired by biological processes are arising as an alternative to standard von-Neumann architectures, to provide hardware accelerators for information processing based on a neural networks approach. Systems of frequency-locked, coupled oscillators are investigated using the phase difference of the signal as the state variable rather than the voltage or current amplitude. As previously shown, these oscillating neural networks can efficiently solve complex and unstructured tasks such as image recognition. We have built nanometer scale relaxation oscillators based on the insulator–metal transition of $VO_2$. Coupling these oscillators with an array of tunable resistors offers the perspective of realizing compact oscillator networks. In this work we show experimental coupling of two oscillators. The phase of the two oscillators could be reversibly altered between in-phase and out-of-phase oscillation upon changing the value of the coupling resistor, i.e. by tuning the coupling strength. The impact of the variability of the devices on the coupling performances are investigated across two generations of devices.

## 1. Introduction

Complex and unstructured problems like speech or image recognition are currently solved most effectively on by *deep learning* algorithms running on specialized electronic circuits such as graphical processing units (GPUs) [1]. The extensive computation effort on these standard von-Neumann computer architectures requires however massive computing resources. This leads to high power consumption which is orders of magnitude higher of today's hardware compared to the human brain when dealing with these tasks. Therefore, alternative, brain-inspired hardware solutions are being researched that can mimic and accelerate the neural network approach of machine learning techniques and perform with lower power consumption [2–4]. Common approaches to build custom neuromorphic hardware are based on spiking artificial neural networks [5–8].

As an alternative approach, Hopfield networks model the physical phenomena of synchronization of oscillators, that comprise associative memory capabilities [9,10]. Weakly coupled oscillators present time-domain characteristics that can be used for computation: the oscillators lock in frequency, while maintaining a fixed phase difference, determined by the weight of the coupling. Changing the coupling strength, this phase relation can be tuned, advancing the possibility of encoding information in the time-domain. The computation capabilities of coupled oscillator systems have been widely demonstrated in literature [11–13,20]. We intend to follow this novel approach as a hardware implementation to perform tasks such as image recognition.

Exploring time domain encoding and information processing is of interest to build a technology that doesn't suffer from scaled power supplies, representing an advantage for the next integrated technology nodes.

Using the phase change material $VO_2$, very compact relaxation oscillators can be fabricated [14]. Previous works obtained stable phase relations in capacitive coupled oscillators [15,16]. In [17] it has been demonstrated that it is possible to build a network that is suitable for performing tasks as image recognition using resistances as coupling elements for the oscillators, envisioning implementation of the coupling with resistive RAM [18]. This would bring to the network the advantage of having reconfigurable weights on chip, allowing online learning of the network

Currently, the best performing oscillators operate at a maximum frequency of 9 MHz [19] and operate at a scaled voltage of 1 V with a power consumption around 10 μW [20]. These results refer to devices build on $TiO_2$ substrate, that being lattice-matched to $VO_2$, allows deposition of crystalline material. It is however technologically relevant

* Corresponding author.
*E-mail address:* sfk@zurich.ibm.com (S. Karg).

https://doi.org/10.1016/j.sse.2019.107729

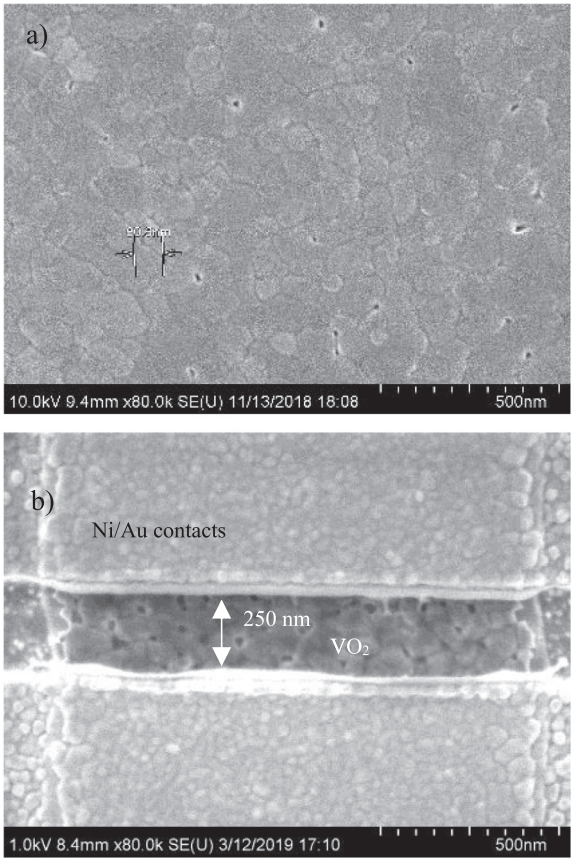


**Fig. 1.** a) SEM image of the $VO_2$ film on $SiO_2$. b) $VO_2$ resistor contacted by two metal electrodes (Ni/Au bilayer). Width and length of the devices were varied from 250 nm to several micrometer.

to develop oscillators on Si, with a process that respect CMOS compatibility. In this work oscillators are built on Si compatible technology on $SiO_2$ substrate, resulting in polycrystalline devices. Two oscillators are coupled with external resistive components, and modulation of the phase relations (in-phase and out-of-phase) is demonstrated upon the tuning of the resistive coupling. The effect of the realization of these devices on Si is explored: it is shown how the variability of the devices resulting from granular films influences the value of the coupling element that is necessary to use to bring the oscillators at the frequency locking condition, and how this impact on the performances of the network.

## 2. Fabrication

The $VO_2$ resistors were realized on a 4″ Si wafer over 1 μm thermal $SiO_2$. The $VO_2$ was deposited with two different techniques, resulting in different film quality. Pulsed Laser Deposition (PLD) was used for devices 1 and 2, and Atomic Layer Deposition (ALD) for devices 3 and 4, targeting a thickness of 50 nm. The ALD devices are annealed at 450 °C for 20 min under oxygen flow, with a partial oxygen pressure of $5{\cdot}10^{-2}$ mbar. Fig. 1 shows an ALD-deposited $VO_2$ film. During the annealing step, grains in the order of 50–80 nm formed in the previously amorphous layer. The film was patterned with ICP etching and contacted with Ni/Au electrodes. The $VO_2$ stripes between the electrodes were are around 250 nm long and 1 μm wide (Fig. 1b). The devices were characterized in vacuum and contacted with a 16-needle probe-card.

Electrical measurements during a temperature sweep were performed to determine the resistivity ratio between the insulating and metallic phase of the two films, and to estimate the width of the

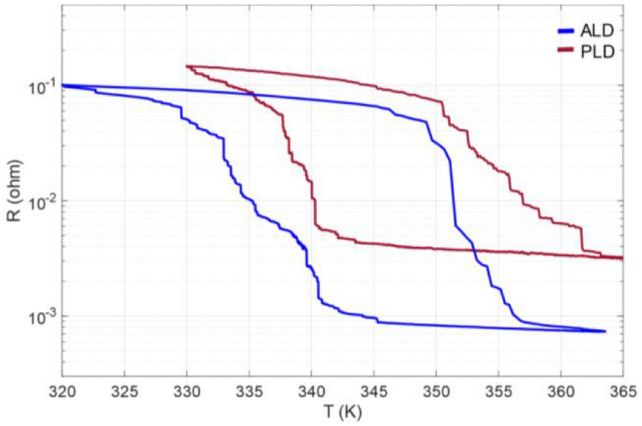


**Fig. 2.** Resistivity comparison of the ALD and PLD samples. The hysteresis plot shows that the phase change in a patterned device is not smooth, but happens in steps.

hysteresis. The phase transition is measured on two devices with equal dimensions, for the devices fabricated with both deposition techniques. The resistivity of a single device is measured in a probe-station equipped with a heating chuck. Extensive resistivity measurements on device level using two-probe and four-probe techniques were taken. An example of the resulting resistivities graph measured on patterned devices is shown in Fig. 2. For the ALD-deposited sample, the average hysteresis width is 18°, with an on–off ratio of two order of magnitude. The PLD-deposited sample has an average resistivity width of 14°, with an on–off ratio of a factor 30. The resistivity values and the width of the hysteresis are comparable to the values already recorded in literature [21]. The insulating to metallic phase change is not smooth but proceeds in defined, reproducible steps that we attribute to transitions of single grains switching inside the devices. The single grain switching is only visible in scaled devices with a low number of grains between the electrodes.

The high and low resistivity values for the PLD and ALD samples result slightly different from each other. Raman analysis of the material was performed for the films, revealing that the films are purely $VO_2$, without contamination from other vanadium oxides stoichiometries. The difference in the resistivity values are attributed to the difference in density of the two films, and the gaps between the grains.

For the ALD devices, each device was conditioned with a forming procedure, consisting of consecutive current sweeps with increasing current range, between 1 μA and 90 μA (Fig. 3). The measurements, executed at 300 K, investigate the electrical excitation of the phase transition via Joule Heating. At a current of around 30 μA (corresponding to a current density in the device of 4 $kA/cm^2$ and a power of 100 μW), the device undergoes a moderate irreversible resistance change. SEM analysis of the device reveal that this irreversible change is correlated with a change of the topology of the device, where neighboring grains fusing together, as reported in Fig. 4. After this forming cycle, subsequent measurements of the devices show that it stabilizes on a reversible phase change.

Evidence of single grain switching is observed similar to the measurements shown in Fig. 2. In fact, two changes in the resistance of the device are measured in the range between 1 μA and 90 μA, associated with different grains phase transitions.

## 3. Experimental results

The basic relaxation-oscillator circuit is depicted in Fig. 5, which shows the circuit configuration for a single oscillator on the top and for two coupled oscillators on the bottom. All the measurements reported in this section were conducted at 300 K. The $VO_2$ resistors (namely $R_{vi}$ in the circuit representation) were connected to external capacitors $C_i$

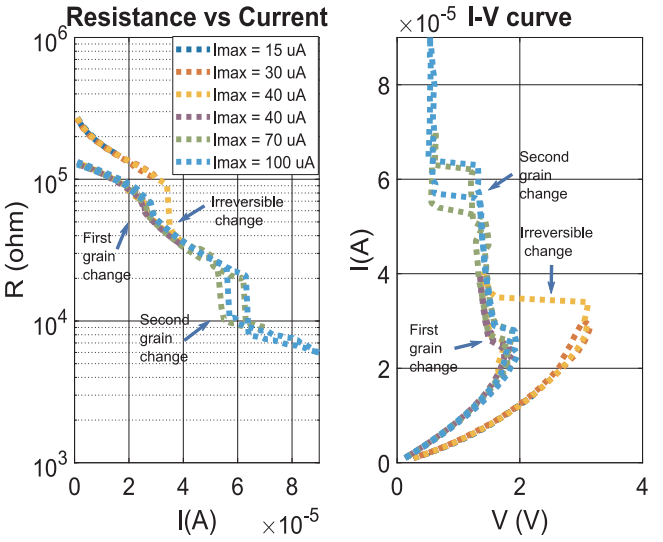


**Fig. 3.** The resistance and I–V characteristics of a $VO_2$ resistor burning cycle. The current was driven through the device and constantly increased. At around 30 μA a first irreversible phase change occurs, that then stabilizes in a minor transition. The real phase change with hysteresis occurs between 60 and 70 μA.

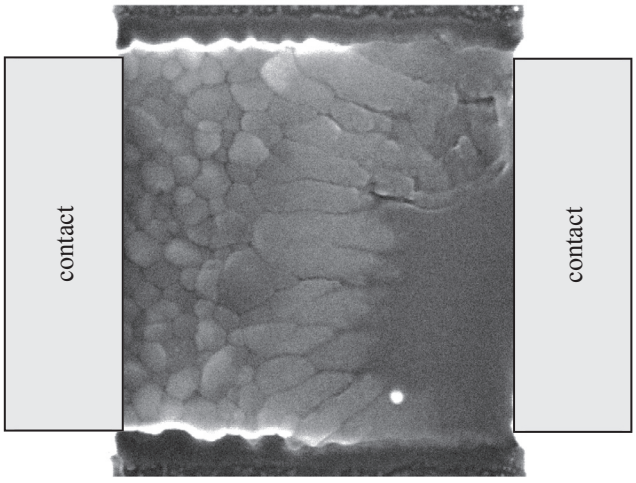


**Fig. 4.** Evidence of grain clustering after the irreversible change of the device upon testing.

and resistors $R_{si}$. The series and coupling resistances $R_{si}$ and $R_c$ are implemented with a variable resistor array (resistor cart National Instrument PXIe-2727). The parallel capacitors $C_i$ was implemented with an external component, and chosen deliberately large (150 nF) to increase the time constant of the circuit and therefore to obtain slower oscillations to comply with the maximum sampling frequency of the set-up.

For a single device, the maximum oscillation frequency that can be obtained is now limited by the parasitic capacitance of the set-up. This limit was explored performing measurements of the oscillation frequency for different values of external capacitances with the current design was also explored. The oscillation period can be described by the Eq. (1):

$$\tau = \tau_r \ln\left(\frac{V_{IN} * H - V_L}{V_{IN} * H - V_H}\right) + \tau_f \ln\left(\frac{V_{IN} * L - V_L}{V_{IN} * L - V_H}\right) \quad (1)$$

Where $\tau_{r,f} = C^*(R_s||R_{ins,met})$, with $R_{ins,met}$ being the insulating and metallic values of the $VO_2$ resistor; H, L = $(R_{ins,met})/(R_{ins,met} + R_s)$; $V_L$, $V_H$ the voltage thresholds for which the device changes its phase. The

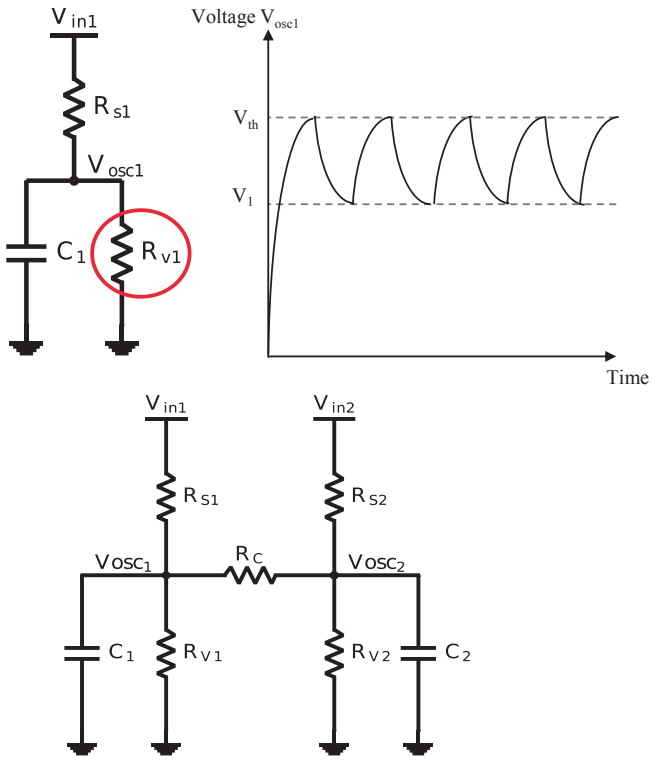


**Fig. 5.** Top: circuit scheme of one relaxation oscillator and corresponding output oscillations. Bottom: circuit scheme of two relaxation oscillators with resistive coupling. Two coupled oscillators represent the basic building block for an Oscillatory Neural Network. The voltages $V_{INi}$ represent the signal inputs to the network. The outputs of the network are the voltages $V_{OSCi}$.

oscillation period is proportional to the capacitance C = ($C_i$ + $C_{par}$), where $C_i$ is the external capacitance, and $C_{par}$ is the parasitic capacitance introduced by the set up. Varying the external capacitor until the point in which the frequency of the oscillations reached its maximum, we could assess that the maximum oscillation frequency obtained with the current device design is of $10^5$ Hz. The parasitic capacitance of our circuitry limits at this point the oscillation frequency: extrapolation of the curve in Fig. 6 gives a value of the parasitic capacitance of around 2 nF. With a fully-integrated circuit we expect the value of the parasitic capacitance to lower and the frequency of oscillation to increase. For scaled, integrated devices the ultimate limit on the oscillation speed is expected to be posed by how fast the device can heat and cool.

Pairs of coupled oscillators from the PLD and ALD batches were investigated. Two $VO_2$ switches with equal dimensions were contacted with external probes. The values for the input voltages $V_1$ and $V_2$ were chosen to establish stable oscillation conditions for the individual $VO_2$ oscillators, while the values of the coupling resistors $R_c$ and self-coupling elements $R_{si}$ were tuned to obtain the different phase conditions of the oscillators. The spontaneous oscillations of a first set of coupled $VO_2$ resonators are shown in Fig. 7 (devices 1 and 2 from PLD deposition). An input voltage of 3.2 V was applied to both oscillators, and the chosen values of the self-coupling elements are $R_{S1}$ = 26 kΩ, $R_{S2}$ = 12 kΩ. Setting the coupling resistors $R_C$ = 3 kΩ leads to in-phase oscillations (Δφ = 1.06°) whereas $R_C$ = 9 kΩ couples the oscillators out-of-phase (Δφ = 179°). The frequencies are 420 Hz for in-phase and 312 Hz for out-of-phase coupling.

For the out-of-phase configuration the shape of the relaxation oscillator presents a double-peak behavior. This is due to the fact that the devices presents quite different resistances and voltage level values ($V_{TH1}$ = 1.9 V, $V_{TL1}$ = 0.77 V, $V_{TH2}$ = 2.2 V, $V_{TL2}$ = 0.67 V for out-of-phase configuration and $V_{TH1}$ = 2 V, $V_{TL1}$ = 0.77 V, $V_{TH2}$ = 2.1 V, $V_{TL2}$ = 1 V for in phase configuration, $R_{V1H}$ = 39.4 kΩ and

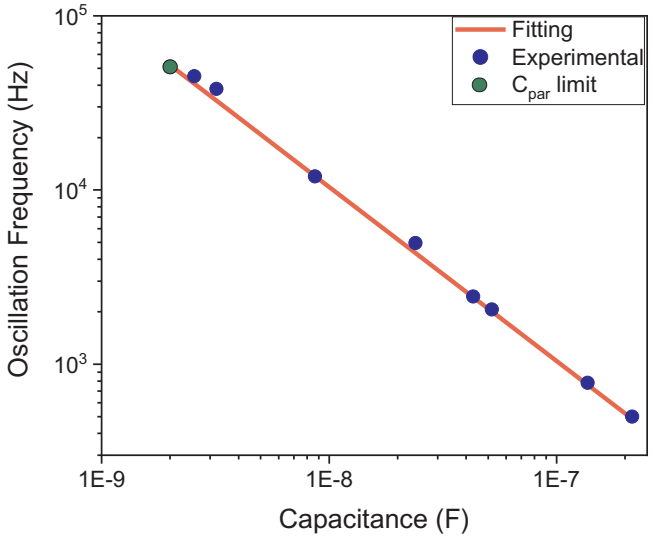


**Fig. 6.** Relation between the oscillation frequency and the capacitance $C = C_i + C_{par}$ (experiments fitted with Eq. (1)). For large values of $C_i$, $C_{par}$ is negligible. For $C_i \ll C_{par}$, the frequency of oscillation stops increasing, allowing an estimation of the parasitic capacitance of $C_{par} = 2$ nF.

$R_{V2H} = 23$ kΩ for the high impedance state and $R_{V1L} = 7.6$ kΩ and $R_{V2L} = 2.8$ kΩ for the low impedance states. The resistances values are calculated respectively before the insulating to metallic and metallic to insulating phase transition. The relative difference in resistance value, calculated as $(R_1\text{-}R_2)/R_{avarage}$ and averaged between the metallic and insulating state, is of 72%. Due to this difference, a rather strong coupling is required to obtain frequency and phase locking of the oscillators.

A strong coupling translates in a smaller value of coupling resistance, that is in this case of the same order of the metallic resistance of the $VO_2$ devices. Upon the phase change of one of the two oscillators, the output voltage of the second oscillator is affected due to the strong correlation between the two outputs.

This causes in the out-of-phase configuration the double peak behavior that can be observed in the output voltage of the oscillators. Ideal waveforms can be obtained when the coupling resistance has a value that is significantly higher than the insulating state of the vanadium oxide resistor. The equivalent resistance to ground calculated at the output of one of the x oscillator ($V_{osc|x}$) nodes is:

$$R_{eqx} = R_{VO|x} \,||\, (R_c + R_{VO|y} || R_{S|y}) \tag{2}$$

and it is insensitive to the transitions of the y oscillator if:

$$R_c >> R_{VOy|insulating}. \tag{3}$$

Moreover, a low value of the coupling resistance translates in a non-negligible current that flows into the coupling element, that therefore contributes significantly to the power consumption of the network, specially in the out-of-phase coupling configuration (with instant power peaks up to 150 μW). Ideally, the coupling element value should be comparable or higher than the insulating state of the $VO_2$ resistor, reducing the oscillation distortion and having negligible power consumption compared to the rest of the network.

Circuit simulation were performed to match the experimental results. The $VO_2$ device was modelled with the equivalent circuit described in [22]. Systematic simulations show that in a network of two coupled oscillators only 2 stable phase conditions exist: either the in-phase or the out-of-phase coupling. Scanning the coupling-resistance parameter space, every intermediate phase relation is converging within 2–3 oscillations to either in-phase or out-of-phase coupling. The simulation moreover shows that for different devices the out-of-phase configuration is the preferred one, while identical devices are more likely to couple in the in-phase configuration.

Coupling of more than two devices is for now limited by the variability of the $VO_2$ switches. Improvements of the film quality has already been achieved with the ALD- deposited films, that reduce the device variability allowing different coupling schemes.

In Fig. 8 the in-phase and out-of-phase coupling of ALD-deposited devices 3 and 4 is shown.

In this case it was necessary to change also the self-coupling

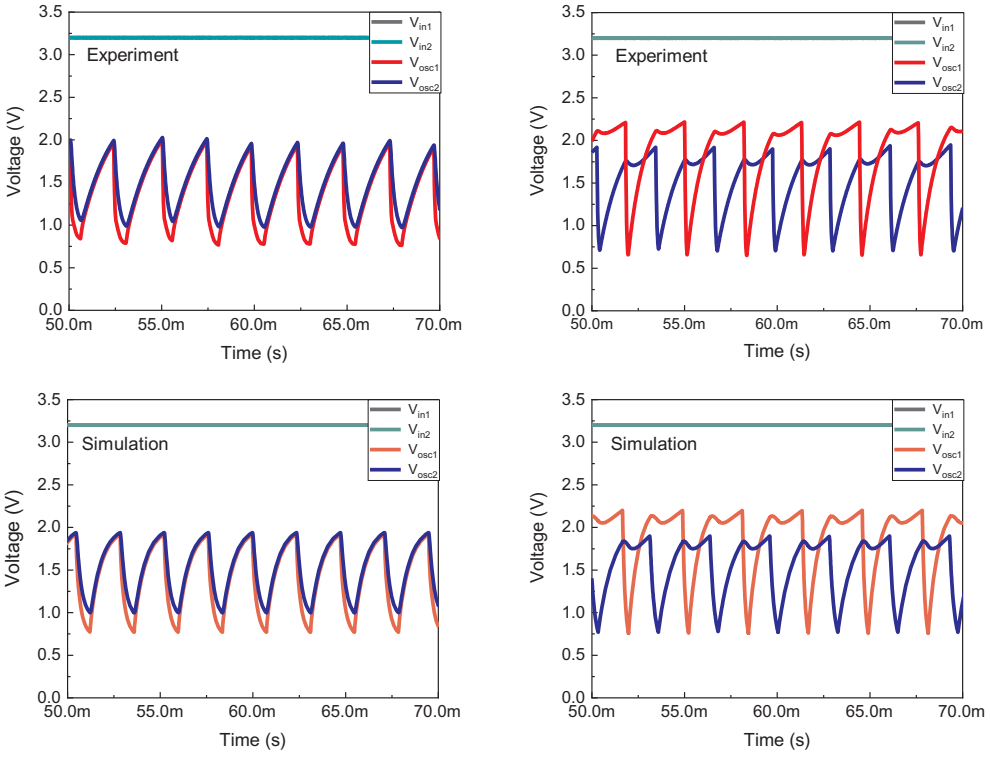


**Fig. 7.** Measured voltage oscillations of coupled $VO_2$ resonators. Changing the value of the coupling resistance, different phase configurations are achieved. $R_C = 3$ kΩ results in in-phase coupling (left), $R_C = 9$ kΩ in out-of-phase coupling (right). Circuit parameters: $V_{in1} = V_{in2} = 3.2$ V, $R_{S1} = 26$ kΩ, $R_{S2} = 12$ kΩ, $C_1 = C_2 = 150$ nF. Bottom: circuit simulation matching the experimental results.

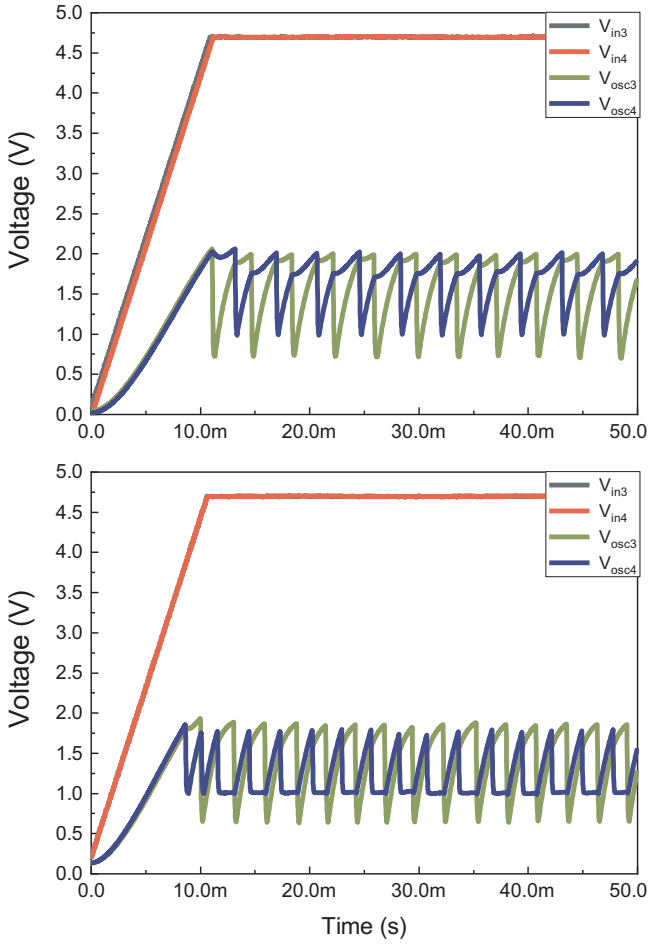


**Fig. 8.** Measured voltage oscillations of coupled Devices 3 and 4. Top: in-phase oscillations. Circuit parameters: $V_{in3} = V_{in4} = 4.7$ V, $C_3 = C_4 = 150$ nF, $R_{S3} = 30$ kΩ, $R_{S4} = 33$ kΩ, Rc = 29 kΩ. Bottom: out-of-phase oscillations. Circuit parameters: $V_{in3} = V_{in4} = 4.7$ V, $C_3 = C_4 = 150$ nF, $R_{S3} = 33$ kΩ, $R_{S4} = 36$ kΩ, Rc = 27 kΩ. The input voltage for ALD devices resulted higher than for the PLD devices; for devices with the same dimensions, this is dependent on the film quality and the details of grain boundaries.

elements, in order to bias the circuit in compliance to the oscillation condition. Details about the circuit parameters are given in Fig. 8. For the ALD prepared films, the devices present similar voltage thresholds for the switching and similar resistances parameters. The reported values of resistances respectively before and after the insulating to metallic transition are: $R_{ins3,4} = 37$–$33.5$ kΩ, $R_{met3,4} = 6$–$4.7$ kΩ. The variation of the devices was greatly improved. The relative difference of the resistances was calculated to be around 15%. Therefore, a less strong coupling is required to lock the oscillators in frequency. Though the coupling resistances were much larger than in the previous example, the double-peak behavior is still observed. In fact, even if it was possible to increase the coupling resistance value of almost an order of magnitude, the value of the coupling resistance is of the order of magnitude of the value of the insulating state of the $VO_2$ resistors upon the transition. Therefore, relation (3) is still not met. However, this result clearly shows that optimizing the devices to achieve more homogeneous properties is essential to reduce the coupling strength of the oscillators, that is an essential step towards the scaling of the network to larger sizes and to exploit the computing capabilities of such a circuit. The figure of merit for devices 1,2 and 3,4 upon coupling are listed in Table 1.

The in-phase configuration of this pair of oscillators looks different than what reported with the PLD devices. A more detailed analysis is required to understand the dynamics that cause this behavior: the first

**Table 1**
List of the Device parameters for the two generation of devices, the PLD and ALD deposited films. The table shows how the reduced variability in the devices characteristic values of insulating and metallic resistance impacts the strength of the coupling that is necessary to lock the oscillators in frequency. From the PLD to the ALD devices, the variability was reduced from 72% to 15%, leading to an increase of the coupling resistance of about a factor 3–10 for the in-phase and out-of-phase oscillations.

**Circuit parameters**

| ALD | In-phase | Out-of-phase |
|---|---|---|
| $V_{in}$ | 4.7 V | 4.7 V |
| $R_{s1}$ | 30 kΩ | 33 kΩ |
| $R_{s2}$ | 33 kΩ | 36 kΩ |
| $R_c$ | 29 kΩ | 27 kΩ |

| PLD | In-phase | Out-of-phase |
|---|---|---|
| $V_{in}$ | 3.2 V | 3.2 V |
| $R_{s1}$ | 26 kΩ | 12 kΩ |
| $R_{s2}$ | 33 kΩ | 36 kΩ |
| $R_c$ | 3 kΩ | 9 kΩ |

**$VO_2$ parameters**

| ALD | $R_{vo3}$ | $R_{vo4}$ |
|---|---|---|
| $V_{TH}$ | 2.1 V | 2 V |
| $V_{TL}$ | 0.9 V | 0.68 V |
| $R_{ins}$ | 37 kΩ | 33.5 kΩ |
| $R_{met}$ | 4.7 kΩ | 7kΩ |

| PLD | $R_{vo1}$ | $R_{vo2}$ |
|---|---|---|
| $V_{TH}$ | 1.9 V | 2.2 V |
| $V_{TL}$ | 0.77 V | 0.67 V |
| $R_{ins}$ | 39.4 kΩ | 23 kΩ |
| $R_{met}$ | 7.6 kΩ | 2.8kΩ |

device changes to the metallic state and the output voltage $V_{osc3}$ stays fixed at a value slightly larger than the threshold voltage $V_{TL2}$, necessary to trigger the metal to insulator transition. The threshold is reached only when the first device also changes its phase, becoming metallic and lowering the voltage partition across the $VO_2$ resistors. The minimum peaks of the two devices are aligned, as shown in the enlargement in Fig. 9: the metal to insulator transition happens in-phase for the coupled oscillators.

Fig. 10 shows a plot of the resistances of the oscillators over time. The data analysis was performed proceeding from the circuit relation of the configuration depicted in Fig. 3 (bottom). From the measured output voltage of the oscillators, the resistance variation over time was calculated as follows:

For obtaining the high impedance state value, additional filtering of the noise through averaging was necessary, due to the resulting small current values.

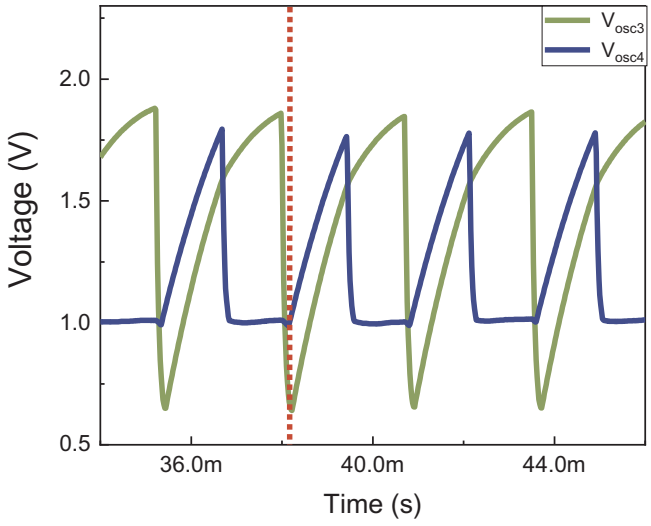


**Fig. 9.** Enlargement of the in-phase oscillations obtained for devices 3 and 4. The minima of the two oscillators is perfectly aligned, therefore giving in-phase coupling of the devices.

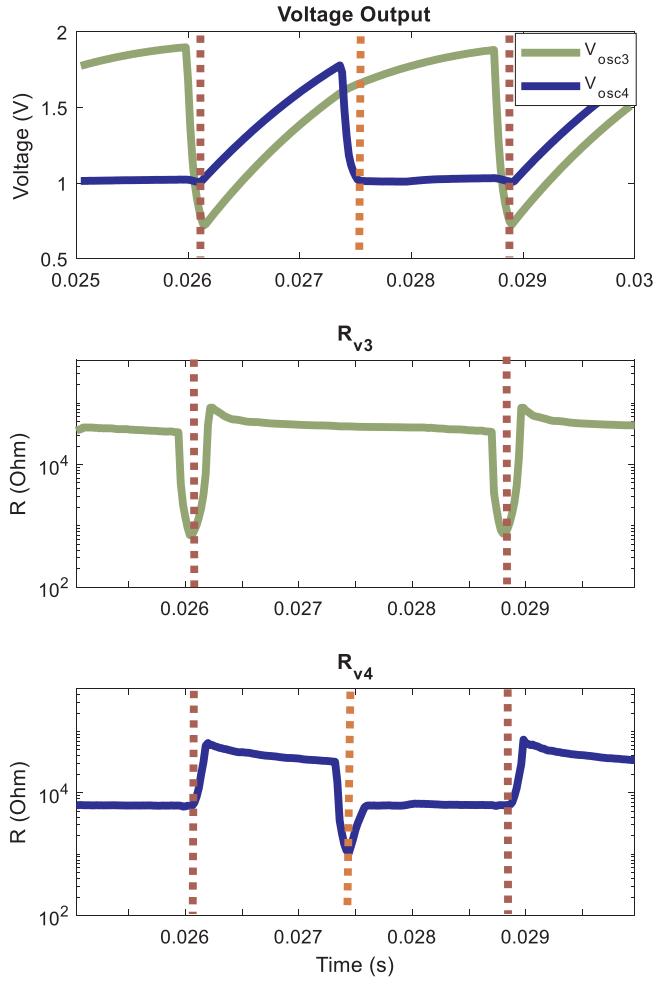


**Fig. 10.** Plot of the resistance of the oscillators over time, for the in-phase coupled oscillators. The rising edges of the oscillations correspond to the insulating phase of the $VO_2$ devices, the falling edges to the conductive phase device 4 stabilizes in two different conductive phases, associated with the switching of different grains at different powers. The metal-to-insulator transition between the two devices is perfectly aligned, defining the in-phase state of the oscillations.

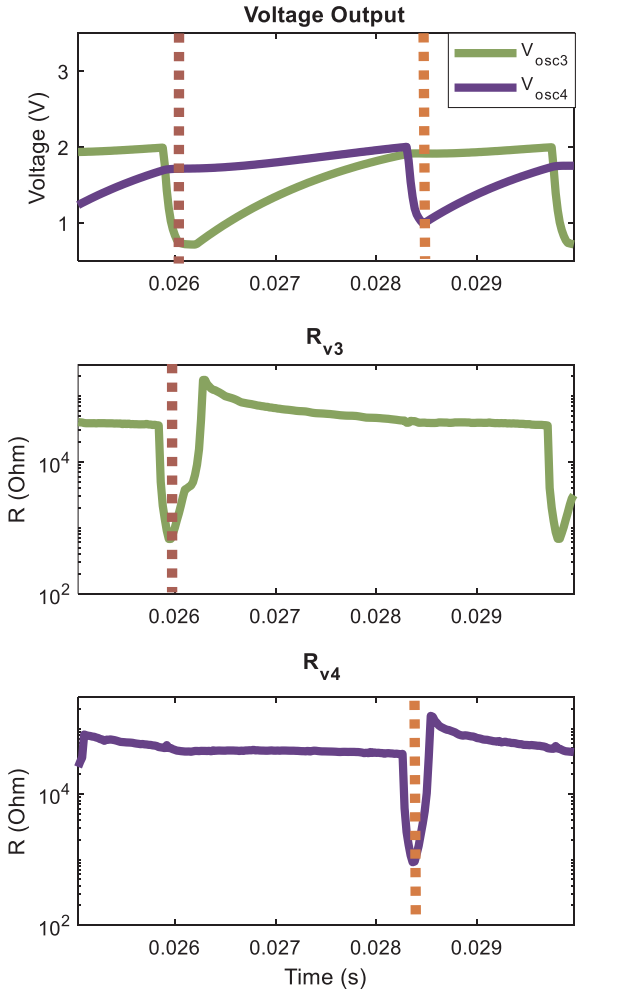


**Fig. 11.** Plot of the resistance of the oscillators over time, for the out-of-phase coupled oscillators. The two devices undergo the metal-to-insulator and the insulator-to-metal transition at different times. In this configuration also device 3 shows two different resistance states, that are visible in the metal-to-insulator transition.

The analysis of the resistance variation over time shows how the rising and falling edges of the oscillators correspond to different resistance states of the vanadium oxide devices. Moreover, it appears clearly during the rising edge that the vanadium oxide insulating resistance of both devices is not constant but spans between values around 100 kΩ and 30 kΩ as the power inside the device increases, in accordance with the I-R characteristic shown in Fig. 2. The same happens when the devices are in the metallic state: their resistances vary depending on the instant power. In this plot it is in addition visible that the low to high transition of the two devices is perfectly aligned, defining the in-phase nature of the coupling. For device 4, two states of low resistivity are reported: at first, when the insulating to metallic phase change occurs, the resistance of the device is reported to be a few 100 Ω, but suddenly it increases and stabilizes to around 7 kΩ. This is attributed at the phase change of different grains inside the materials at high current values.

Two different low resistance states are reported also for device 3, but are visible only in the out-of-phase configuration, upon the analysis of the resistance values over time. Fig. 11 shows again the resistance over time variation of the two oscillators. In the middle graph, the resistance of the device 3 presents an additional jump between a few Ohm resistance value and the 4.7 kΩ value before the metallic-to-insulating phase transition.

## 4. Conclusion

Highly scalable electrical relaxation-oscillators can be built using $VO_2$ metal–insulator switches. If connected with electrical components, the oscillators show frequency and phase-locking properties, that can be used for computing. In this paper we investigated the properties of $VO_2$ coupled oscillator fabricated on a Si substrate. We experimentally showed frequency and phase-locking of $VO_2$ on Si resistively-coupled oscillators. With experiments and circuits simulations we achieved control of the phase relation between the two oscillators using variable resistors. Oscillators were built using different $VO_2$ films, obtained with PLD and ALD deposition on a $SiO_2$ substrate. The devices build with both techniques were compared in their coupling capabilities. For the PLD devices, in-phase and out-of-phase coupling was obtained despite the significant variability between the devices. As the device's variability increases, a stronger coupling is necessary to obtain frequency-locking. For the ALD devices the variability was greatly reduced, allowing use an order of magnitude weaker coupling strength to achieve frequency-locking. Both devices exhibited distorted patterns in the out-of-phase configuration, that has been linked with the relative value of the coupling resistance compared to the value of the insulating state of the $VO_2$ devices upon phase change. Analysis of the impact of ultra-

scaled devices on the waveform of the oscillators was performed. Due to the discrete number of single grains, individual switching events mask the electrical characteristics of oscillators. Oscillators still couple in phase and out of phase upon the tuning of the coupling element but can show different oscillating patterns in relation to the phase change steps that occur across the devices. This doesn't impact the phase relation that it is possible to establish between two oscillators. The control of the output phase-relation with the tuning of the coupling element is in fact ultimately retained in the $VO_2$ on Si devices, despite the grain-size effects and the variability in the device characteristics, demonstrating the potential for this technology to achieve Si-compatibility and to be employed for dedicated hardware for neuromorphic computing. Ultimately, improvements of the $VO_2$ film quality are required to obtain more similar oscillators and to allow the scaling of the network to larger sizes.

## Acknowledgments

This work has been supported by the HORIZON 2020 PHASE-CHANGE SWITCH Project (Grant. No. 737109).

## References

[1] LeCun Y, Bengio Y, Hinton G. Deep learning. Nature 2015;521:436–44.
[2] Indiveri G, Liu SC. Memory and information processing in neuromorphic systems. Proc IEEE 2015;103(8):1379–97.
[3] Tsai H, Ambrogio S, Narayanan P, Shelby RM, Burr GW. Recent progress in analog memory-based accelerators for deep learning. J Phys D: Appl Phys 2018;51:283001.
[4] Burr GW, et al. Neuromorphic computing using non-volatile memory. Adv Phys X 2017;2(1):89–124.
[5] Indiveri G, Linares-Barranco B, Hamilton TJ, Van Schaik A, Etienne-Cummings R, Delbruck T, et al. Neuromorphic silicon neuron circuits. Front Neurosci 2011;5:73.
[6] Merolla PA, et al. A million spiking-neuron integrated circuit with a scalable communication network and interface. Science 2014;345(6197):668–73.
[7] Painkras E, et al. SpiNNaker: a 1-W 18-core system-on-chip for massively-parallel neural network simulation. IEEE J Solid-State Circuits 2013;48:1943–53.
[8] Qiao N, et al. A reconfigurable on-line learning spiking neuromorphic processor comprising 256 neurons and 128K synapses. Front Neurosci 2015;9:141.
[9] Hoppensteadt F, Izhikevich E. Oscillatory neurocomputers with dynamic connectivity. Phys Rev Lett 1999;82:2983–6.
[10] Izhikevich E. Computing with oscillators. Neural Networks 2000;5255:1–30.
[11] Raychowdhury A, et al. Computing with networks of oscillatory dynamical systems. Proc IEEE 2019;107(1):73–89.
[12] Jerry M, Ni K, Parihar A, Raychowdhury A, Datta S. Stochastic insulator-to-metal phase transition-based true random number generator. IEEE Electron Device Lett 2018;39(1):139–42.
[13] Parihar, Shukla N, Jerry M, Datta S, Raychowdhury A. Computing with dynamical systems based on insulator-metal-transition oscillators. Nanophotonics 2017;6(3):601–11.
[14] Shukla N, et al. Synchronized charge oscillations in correlated electron systems. Sci Rep 2015;4(1):4964.
[15] Parihar A, Shukla N, Datta S, Raychowdhury A. Synchronization of pairwise-coupled, identical, relaxation oscillators based on metal-insulator phase transition devices: a model study. J Appl Phys 2015;117(5).
[16] Perminov VV, Putrolaynen VV, Belyaev MA, Velichko AA. Synchronization in the system of coupled oscillators based on VO2 switches. J Phys Conf Ser 2017;929(1):12045.
[17] Corti E, Gotsmann B, Moselund K, Stolichnov I, Ionescu AM, Karg S. Resistive coupled VO2 oscillators for image recognition 2018; 1–7. 10.1109/ICRC.2018.8638626.
[18] Boybat I, et al. Neuromorphic computing with multi-memristive synapses. Nat Commun 2018;9(1):2514.
[19] Mian MS, Okimura K, Sakai J. Self-oscillation up to 9 MHz based on voltage triggered switching in $VO_2$/TiN point contact junctions. J Appl Phys 2015;117(21):215305.
[20] Dutta S, et al. Programmable coupled oscillators for synchronized locomotion. Nat Commun 2019;10(1):3299.
[21] Peter AP, et al. Metal-insulator transition in ALD $VO_2$ ultrathin films and nanoparticles: morphological control. Adv Funct Mater 2015;25:679–86.
[22] Maffezzoni P, Daniel L, Shukla N, Datta S, Raychowdhury A. Modeling and simulation of vanadium dioxide relaxation oscillators. IEEE Trans Circuits Syst I Regul Pap 2015;62(9):2207–15.